Vacuum 101 (2014) 10–17

Contents lists available at ScienceDirect

Vacuum

journal homepage: www.elsevier.com/locate/vacuum

Rarefied gas flow through a diverging conical pipe into vacuum

V.A. Titarev [a,b,*], E.M. Shakhov [c], S.V. Utyuzhnikov [d,b]

[a] Dorodnicyn Computing Centre of Russian Academy of Sciences, Moscow, Russia
[b] Moscow Institute of Physics and Technology, Moscow, Russia
[c] Bauman Moscow State Technical University, Moscow, Russia
[d] University of Manchester, Manchester, UK

ARTICLE INFO

Article history:
Received 6 April 2013
Received in revised form
12 July 2013
Accepted 17 July 2013

Keywords:
Rarefied
Kinetic
S-model
Conical pipe
Vacuum
Computational physics

ABSTRACT

The paper is devoted to the study of a rarefied gas flow through a finite length conical pipe into vacuum. The problem is solved in the complete geometrical setup, which included not only the pipe, but also high- and low-pressure reservoirs. The analysis is based on the direct numerical solution of the Boltzmann kinetic equation with the S-model collision integral in three space dimensions. The method of the solution is based on the recent implicit total variation diminishing (TVD) method on unstructured spatial meshes. It is conservative with respect to the collision integral and work across all flow regimes. The results are provided for various ratios of the outlet and inlet diameters, pipe's lengths and Knudsen numbers. The computed flow rates are compared with the case of the circular pipe of constant radius as well as an approximate method for very long pipes. The influence of the pipe geometry on the flow field is also examined. The presented results can be used as a benchmark for calculations by other methods and codes.

1. Introduction

A rarefied gas flow through a finite-length pipe or capillary into vacuum is a popular problem in the rarefied gas dynamics [1,2]. The majority of the computational studies deal with the flow through a circular pipe with the constant cross sectional area. Examples include the Direct Simulation Monte Carlo (DSMC) studies for short tubes [3] and deterministic studies for short, moderate and long pipes [4–6]. A comparison of the results from different approaches with experimental data for the short tube can be found in [7].

It is important that all cited studies analyse the problem in the complete setup, which includes not only the pipe, but also high and lower pressure reservoirs, rather than a simplified formulation, in which the reservoirs are replaced by the evaporation and/or condensation boundary conditions at the pipe's ends [8,9]. It appears that the such a setup, albeit in the planar case, was first considered in [10,11]. The influence of the geometrical setup on the flow rate for circular pipe flow was investigated in detail in [5,6].

However, there seem to be no results in the literature for the rarefied gas flow into vacuum through a conical pipe. If one is only interested in the mass flow rate and density distribution along the axial line of the pipe, an approximate method [12,13] can be used. However, it is valid for very long pipes only, for which the ratio of both inlet and outlet radii to the length is small. Moreover, the analysis presented in [4–6] shows that for small Knudsen numbers this condition along is not enough and that the product of the Knudsen number and the pipe length has to be large for the approximate method to be applicable.

The present work is devoted to the deterministic kinetic study of the rarefied gas flow into vacuum through moderate and long conical pipes and can thus be viewed as a continuation of [4–6]. The results are based on the numerical solution of the S-model kinetic equation [14–16] using the recent three-dimensional finite-volume method [17,18]. The computations are carried out for various length and outlet to inlet diameter ratios across the range of rarefaction conditions from the free-molecular to nearly continuum flow regimes. Numerical results for the mass flow rate and distribution of macroscopic macroparameters are presented in the broad range of Knudsen numbers, pipe's length and outlet to inlet radii ratios. The influence of the pipe geometry on the flow rate and distribution of macroscopic quantities is examined.

2. Formulation of the problem

The formulation of the problem is an extension of [3–6]. Consider a rarefied gas flow through a conical pipe of length L,

* Corresponding author. Dorodnicyn Computing Centre of Russian Academy of Sciences, Moscow, Russia.
E-mail addresses: titarev@ccas.ru, vladimirot@yandex.ru (V.A. Titarev), shakhov@ccas.ru (E.M. Shakhov), s.utyuzhnikov@manchester.ac.uk (S.V. Utyuzhnikov).

0042-207X/$ – see front matter © 2013 Elsevier Ltd. All rights reserved.
http://dx.doi.org/10.1016/j.vacuum.2013.07.030

connecting two infinitely large reservoirs (volumes) filled with the same monatomic gas. The inlet and outlet radii of the pipe are denoted as aR_1, R_2, respectively. The gas in the left reservoir is kept under pressure p_1 and temperature T_1, whereas in the right reservoir the pressure is p_2 is so low that it can be regarded as equal to zero. It is assumed that reservoirs' volumes are significantly larger than the pipe volume and the gas is in equilibrium far away from the ends of the latter. The real form and size of the reservoirs are thus of no importance. The complete accommodation of momentum and energy of molecules occurs at the pipe surface, which is kept under the same constant temperature T_1.

Let us introduce a Cartesian coordinate system (x,y,z) with the centre located in the centre of the inlet section of the pipe $x = y = z = 0$ and the Oz axes directed along the tube. A steady three-dimensional state of the rarefied gas is determined by the velocity distribution function $f(\boldsymbol{x},\boldsymbol{\xi})$, where $\boldsymbol{x}=(x,y,z)$ is the spatial coordinate, $\boldsymbol{\xi}=(\xi_x,\xi_y,\xi_z)$ is the molecular velocity vector. For the rest of the paper, the non-dimensional formulation is used, in which the spatial coordinates $\boldsymbol{x}$, mean velocity $\boldsymbol{u} = (u_1,u_2,u_3) = (u_x,u_y,u_z)$, number density n, temperature T, heat flux vector $\boldsymbol{q} = (q_1,q_2,q_3)$, viscosity μ and distribution function f are scaled using the following quantities:

$$R_1, \quad \beta, \quad n_1, \quad T_1, \quad mn_1\beta^3, \quad \mu_1 = \mu(T_1), \quad n_1\beta^{-3}, \tag{1}$$

where $\beta = \sqrt{2kT_1/m}$; $n_1 = p_1/kT_1$ is the number density in the left reservoir; m is the mass of a molecule, k is the Boltzmann constant. Below, the non-dimensional variables are denoted by the same letters as the dimensional ones.

The distribution function f is assumed to satisfy the S-model kinetic equation [14–16], which in the non-dimensional variables takes the form

$$\begin{gathered}
\xi_x\frac{\partial f}{\partial x}+\xi_y\frac{\partial f}{\partial y}+\xi_z\frac{\partial f}{\partial z} = \nu\left(f^{(S)}-f\right), \quad \nu = \frac{nT}{\mu}\delta_1, \quad \delta_1 = \frac{R_1 p_1}{\mu_1\beta}, \\
f^{(S)} = f_M\left[1+\frac{4}{5}(1-\mathrm{Pr})S_\alpha c_\alpha\left(c^2-\frac{5}{2}\right)\right], \quad f_M = \frac{n}{(\pi T)^{3/2}}\exp\left(-c^2\right), \\
v_i = \xi_i - u_i, \quad c_i = \frac{v_i}{\sqrt{T}}, \quad S_i = \frac{2q_i}{nT^{3/2}}, \quad c^2 = c_\alpha c_\alpha.
\end{gathered} \tag{2}$$

Here δ_1 is the so-called rarefaction parameter, which is inversely proportional to the Knudsen number. Summation over repeated Greek indices is assumed. For a monatomic gas the Prandtl number $Pr = 2/3$. The non-dimensional macroscopic quantities are defined as the integrals of the velocity distribution function with respect to the molecular velocity:

$$\begin{gathered}
\left(n, n\boldsymbol{u}, n\left(\tfrac{3}{2}T+u^2\right), \boldsymbol{q}\right) = \int\left(1,\boldsymbol{\xi},\xi^2,\frac{1}{2}\boldsymbol{v}v^2\right)f d\boldsymbol{\xi}, \\
u^2 = u_\alpha u_\alpha, \quad v^2 = v_\alpha v_\alpha, \quad \xi^2 = \xi_\alpha\xi_\alpha, \quad p = nT.
\end{gathered} \tag{3}$$

The kinetic equation (2) has to be augmented with the boundary conditions on the pipe and reservoir walls. Let $\boldsymbol{n} = (n_x,n_y,n_y)$ be the unit normal vector to a boundary surface, pointing inside the flow domain. The condition of diffuse molecular scattering on the pipe surface with complete thermal accommodation to the non-dimensional surface temperature $T_1 \equiv 1$ is given by:

$$f(\boldsymbol{x},\boldsymbol{\xi}) = f_w = \frac{n_w}{(\pi)^{3/2}}\exp\left(-\xi^2\right), \quad \xi_n = (\boldsymbol{\xi},\mathbf{n}) > 0. \tag{4}$$

The density of reflected molecules n_w is found from the impermeability condition stating that the mass flux through the walls is equal to zero:

$$n_w = N_i/N_r, \quad N_i = -\int\limits_{\xi_n<0}\xi_n f d\boldsymbol{\xi}, \quad N_r = \int\limits_{\xi_n>0}\xi_n\frac{1}{(\pi)^{3/2}}\exp\left(-\xi^2\right)d\boldsymbol{\xi}. \tag{5}$$

The same condition (5) is used for the parts of the reservoir walls directly adjacent to the pipe; these are located at $z = 0,L$. At the rest of the reservoir wall the distribution function of the incoming molecules $\xi_n > 0$ is specified as

$$\begin{gathered}
f = f_1 = \frac{n_1}{(\pi)^{3/2}}\exp\left(-\xi^2\right), \quad z \le 0, \\
f = 0, z \ge L.
\end{gathered} \tag{6}$$

The boundary condition (6) is essentially an evaporation boundary condition for the molecules entering the flow domain and is meant to model the indefinitely large reservoirs.

The main computed characteristic of the flow is the mass flow rate M, which in the non-dimensional variables is given by an integral over the cross section:

$$\dot{M} = \int\limits_{A(z)}\rho(x,y,z)u_z(x,y,z)dxdy. \tag{7}$$

Here $A(z)$ is the cross-sectional area at the position z along the pipe. Note, that mass flow rate $\dot{M}$ is constant along the pipe.

3. Details of the calculations

3.1. Method of solution

The formulated problem possesses the cylindrical symmetry and can thus be solved in the cylindrical coordinate system. However, our experience suggests that the direct three-dimensional solution methods are more accurate and efficient than the approaches based on the axisymmetrical formulations. In the present work the steady-state solution of the problem is found by means of an implicit time-marching algorithm for the kinetic equation (2) in the non-stationary form. The numerical method consists of the high-order accurate advection scheme applicable to hybrid unstructured meshes, conservative procedure for the calculation of the model collision integral and one-step implicit time evolution for fast steady-state convergence. As a result, it allows efficient calculation of rarefied flows in the wide range of degrees of rarefaction in arbitrary geometries.

A summary of the numerical method can be found in [18], see also [17,19] and references therein. The infinite domain of integration in the molecular velocity space is replaced by a finite computational domain. The velocity distribution function is then defined in centres of the resulting velocity mesh. The kinetic equation (2) is replaced by a system of time-dependent advection equations; each equation corresponds to a specific point from the velocity mesh. The macroscopic quantities at any spatial location are computed in such a way as to satisfy not only conservation laws, but also correct relaxation of the heat flux vector. Assuming the model collision integral is known, the equations are solved using an implicit TVD method, which is second-order accurate in space. An LU-SGS type time evolution procedure on unstructured meshes [20] is used to allow for faster steady-state convergence.

For large-scale problems such as the ones reported here the calculations are carried out on modern high-performance clusters using Message Passing Interface (MPI). In the present work the HPC "Lomonosov" of Lomonosov Moscow State University, Russia, was utilized. The runs were performed on up to 160 cores of the

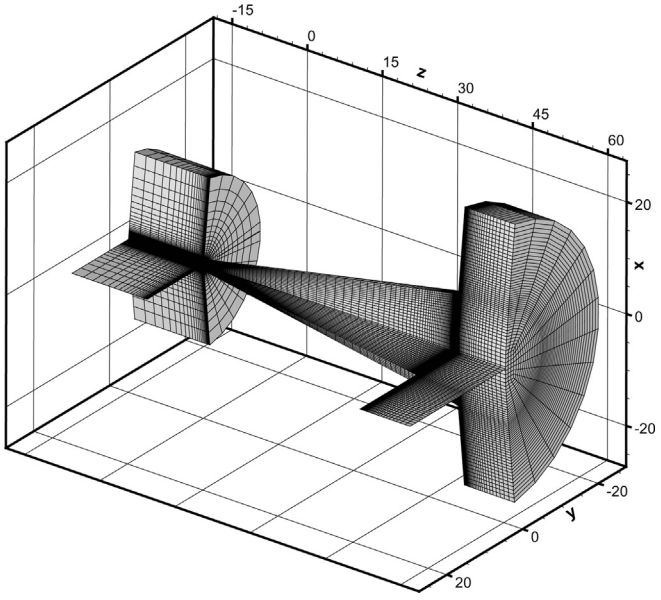

Fig. 1. Crossectional views of the spatial mesh; $L/R_1 = 50$, $R_2/R_1 = 10$, 116 thousands cells.

machine (40 CPUs) depending on the mesh resolution, pipe length, R_2/R_1 ratio and the value of the rarefaction parameter δ_1.

3.2. Choice of spatial and velocity meshes

Special attention was given to the accuracy of calculations, which for the fixed second-order TVD discretization scheme is influenced by the spatial and velocity mesh resolutions and domain sizes. The solution of the problem for three considered length to radius ratios L/R_1 and many values of the rarefaction parameter δ requires a huge amount of six-dimensional calculations. It is thus impossible to carry out a detailed convergence study in the six-dimensional space $(\boldsymbol{x},\boldsymbol{\xi})$ in order to determine the optimal resolution of spatial and velocity meshes. Instead a limited number of convergence runs is performed for a carefully selected set of conditions, and the estimated mesh resolutions and sizes are then used for the main bulk of calculations.

All calculations are run on purely hexahedral spatial meshes. The definition of the parameters of the spatial mesh begins with the estimation of the required size of the reservoirs. The use of small domains for reservoirs decreases the computational effort required to obtain the solution, but may lead to the underestimation of the mass flow rates. In particular, the spatial domain modelling the high-pressure reservoir must be sufficiently large. It was found that for the accurate calculation of the mass flow rate the use of the reservoir 1 of dimensions 10 units length and 10 units radius is adequate for most of the cases. For $R_2/R_1 \geq 5$ the size of the reservoir 1 is increased to be the cylinder of 15 units length and radius. The size of the reservoir 2 is less important as the flow becomes supersonic. In order to calculate the flow pattern in the vacuum region the radius of the reservoir 2 is set to $R_2 + 15 \ldots R_2 + 20$ units whereas the length is 5–10 units.

The distribution function in the problem in hand is discontinuous and varies sharply in the certain areas of the flow. To resolve sharp gradients, the spatial mesh is clustered towards the pipe surface as well as inlet and outlet surfaces. The cell size normal to the inlet and outlet positions was usually equal to $h_{i,o} = 0.03 \ldots 0.05$ units. The mesh resolution normal to the surface varied linearly with the radius of the pipe as $h_n(z) = 0.03 \cdot R(z)$, where $R(z)$ is the pipe radius at the position $0 \leq z \leq L$. The total number of spatial cells varies depending on the R_2/R_1 ratio and is at the level of 90–110 thousands. A typical spatial mesh for $L/R_1 = 50$ and $R_2/R_1 = 10$ is shown on Fig. 1.

The integration domain in the velocity space was a cylinder, see Fig. 8 of [19]. In this work it is of radius 4 and length 8, with the axis coinciding with the pipe's axis. The cylindrical velocity mesh consisted of 25 cells in the radial direction, 16 cells in the angular direction and 20…40 cells in the z direction. The radial component of the mesh was clustered towards the origin. The velocity mesh resolution for mass flow rate calculations can be deemed sufficient because the most difficult case of the free-molecular flow $\delta_1 = 0$ is computed accurately.

The numerical solution is considered converged to the steady state once the residual in the integral conservation laws drops several orders of magnitude and the time derivative of the flow rate becomes negligible. Calculations show that it is much more difficult to obtain a formal steady-state convergence of the solution for the conical geometry as compared to the case of the cylindrical pipe. It should also be noted that in all calculations the deviation of the

Table 1
Flow rate Q for $L/R_1 = 1$ and various R_2/R_1 ratios.

δ_1	$R_2/R_1 = 1$			1.1	2
	Ref. [3]	Ref. [4]	Present	Present	Present
0.	0.672	0.670	0.671	0.742	0.976
0.1	0.680	0.681	0.683	0.757	0.996
1.	0.754	0.758	0.766	0.851	1.123
5.	0.948	0.949	0.953	1.055	1.352
10.	1.062	1.058	1.061	1.175	1.438
20.	1.168	1.161	1.164	1.280	1.489
30.			1.220	1.332	1.507
50.	1.287	1.281	1.282	1.390	1.518
100	1.358	1.355	1.352	1.448	1.522

Table 2
Flow rate Q for $L/R_1 = 1$ and various R_2/R_1 ratios.

δ_1	$R_2/R_1 = 1$		1.1	2	5
	Ref. [3]	Present	Present	Present	Present
0.	0.311	0.309	0.350	0.644	0.958
0.1	0.312	0.313	0.354	0.655	0.976
1.	0.334	0.339	0.386	0.734	1.098
5.	0.436	0.439	0.505	0.973	1.338
10.	0.543	0.544	0.615	1.133	1.437
20.	0.695	0.693	0.774	1.290	1.496
30.		0.792	0.874	1.358	1.522
50.	0.917	0.916	0.992	1.417	1.537
100	1.068	1.071	1.127	1.464	1.545

Table 3
Flow rate Q for $L/R_1 = 10$ and various R_2/R_1 ratios.

δ_1	$R_2/R_1 = 1$			1.1	2	5	10
	Ref. [3]	Ref. [4,6]	Present	Present	Present	Present	Present
0.	0.192	0.190	0.190	0.216	0.436	0.833	0.977
0.1	0.190	0.190	0.191	0.217	0.441	0.845	1.000
1.	0.198	0.199	0.201	0.230	0.483	0.957	1.121
5.	0.258	0.258	0.261	0.302	0.657	1.212	1.359
10.	0.335	0.335	0.335	0.390	0.839	1.347	1.445
20.	0.463	0.462	0.462	0.537	1.076	1.445	1.502
30.			0.559	0.649	1.202	1.481	1.527
50.	0.696	0.697	0.697	0.804	1.329	1.504	1.540
100	0.874	0.888	0.889	1.010	1.432	1.533	1.547

Table 4
Flow rate Q for $L/R_1 = 20$ and various R_2/R_1 ratios.

δ_1	$R_2/R_1 = 1$		1.1	2	5	10
	Ref. [4,6]	Present	Present	Present	Present	Present
0.	0.108	0.108	0.124	0.264	0.611	0.859
0.1	0.107	0.108	0.123	0.265	0.620	0.876
1.	0.110	0.111	0.127	0.281	0.692	0.987
5.	0.144	0.143	0.166	0.385	0.932	1.234
10.	0.187	0.188	0.220	0.517	1.132	1.365
20.	0.272	0.272	0.320	0.743	1.315	1.453
30.		0.347	0.408	0.907	1.388	1.486
50.	0.469	0.469	0.550	1.110	1.450	1.512
100	0.667	0.667	0.773	1.317	1.498	1.530

mass flow rate value $\dot{M}$ from constant value is small and does not exceed 1.5% for the most difficult case $R_2/R_1 = 10$. By default, the value of $\dot{M}$ corresponding to the middle section of the pipe is used in the presentation of results.

4. Results

4.1. Flow rate

The solution of the problem depends on the rarefaction parameter δ_1, the length to the inlet radius ratio L/R_1 as well as outlet to inlet radii ratio R_2/R_1. The calculations are run for the length to radius ratios $L/R_1 = 1$, 5, 10, 20, 50 and various values of outlet to inlet ratios $R_2/R_1 = 1$, 1.1, 2, 5 and 10. In all cases the radius of the outlet is such that $R_2/L \le 1$. The rarefaction parameter values varied in the range $0 \le \delta_1 \le 100$ and covered the flow regimes from the free-molecular to nearly-hydrodynamic one.

In the presentation of the results, the reduced mass flow rate Q is used instead of the conventional mass flow rate [8,3]. The value of Q is defined as the ratio of the mass flow rate $\dot{M}$ at given δ_1, L/R_1 and R_2/R_1 to the value $\dot{M}_0$ corresponding to the free-molecular flow through the orifice of radius R_1:

$$Q = \frac{\dot{M}}{\dot{M}_0}, \quad \dot{M}_0 = \frac{\sqrt{\pi}}{2}. \tag{8}$$

Tables 1–5 contain the data on the reduced flow rate Q as a function of all flow parameters: δ_1, L/R_1, R_2/R_1. For the case of constant cross sectional area also included are the DSMC values from Ref. [3] as well as earlier deterministic calculations [4,6] on a finer spatial mesh. There is a generally good agreement between all three sets of results for $R_2/R_1 = 1$ with the discrepancy well within the computational error of calculations. It should also be noted that accurate DSMC calculations of the monatomic gas flow may be considered as equivalent to the direct solution of the Boltzmann kinetic equation with the exact collision integral. The S-model kinetic equation is only an approximation to the latter equation, devised to be exact for the free-molecular flow $\delta_1 = 0$ and very accurate for continuum regime $\delta_1 \gg 1$. In case of intermediate values of the Knudsen number a certain (usually small) discrepancy between exact and model equations is expected, which should be taken into consideration while analysing the results, presented in Tables 1–5.

Table 5
Flow rate Q for $L/R_1 = 50$ and various R_2/R_1 ratios.

δ_1	$R_2/R_1 = 1$		1.1	2	5	10
	Ref. [4,6]	Present	Present	Present	Present	Present
0.	0.047	0.047	0.054	0.121	0.331	0.568
0.1	0.046	0.047	0.054	0.121	0.334	0.576
1.	0.047	0.047	0.055	0.124	0.355	0.638
5.	0.060	0.060	0.071	0.169	0.497	0.871
10.	0.079	0.080	0.094	0.233	0.673	1.080
20.	0.119	0.120	0.141	0.360	0.944	1.281
30.		0.158	0.187	0.477	1.110	1.363
50.	0.228	0.230	0.273	0.674	1.275	1.431
100	0.379	0.378	0.447	0.990	1.408	1.484

Table 6
Comparison of flow rate M_p and approximation (11) for $R_2/R_1 = 1.1$, 2.

	$R_2/R_1 = 1.1$				$R_2/R_1 = 2$			
δ_1	$L/R_1 = 10$	20	50	Eq. (11)	$L/R_1 = 10$	20	50	Eq. (11)
0.	1.217	1.393	1.533	1.734	2.446	2.974	3.424	4.013
0.1	1.226	1.390	1.521	1.659	2.477	2.985	3.406	3.823
1.	1.295	1.431	1.537	1.637	2.712	3.174	3.501	3.801
10.	2.196	2.475	2.654	2.804	4.715	5.837	6.575	7.110
100	5.698	8.723	12.62	16.31	8.086	14.85	27.88	45.49

The flow rate increases as the outlet radius grows. For the small change in the outlet radius ($R_2/R_1 = 1.1$ or 10%) for any value of the rarefaction parameter δ_1 in the considered range the values of flow rate Q can be computed from the circular pipe data:

$$Q(R_2/R_1 = 1.1,\ \delta_1) \approx 1.15 \cdot Q(R_2/R_1 = 1, \delta_1) \tag{9}$$

which can be considered as a linear dependence on $\delta R = R_2/R_1 - 1$. However, for larger difference in radii $R_2/R_1 \ge 2$ the flow rate departure from the circular pipe is nonlinear and cannot be described by a fixed multiplication coefficient. The growth of the flow rate with the increase of the outlet radius is explained by fact that diverging surface of the conical pipe poses smaller resistance to the flow as compared to the circular pipe. It is expected that the further increase in R_2/R_1 ratio will result in even larger flow rate values. The upper limit is provided by the orifice flow.

4.2. Comparison with the approximate method

The computed values of the flow rate can be used to assess the accuracy of the approximate method [12,13] for the case of conical pipes. For the constant cross section circular pipe such an analysis was carried out in [4–6]. It was shown that the approximate method is restricted to the flow regimes satisfying the condition $\delta_1(R_1/L) \ll 1$.

Consider another reduced flow rate:

$$M_p = \frac{2}{A}\frac{1}{K_p}\dot{M}, \quad K_p = \frac{p_1}{L}, \tag{10}$$

where A is cross sectional area of the inlet section of the pipe, K_p can be regarded as the mean pressure gradient. The approximate method [12,13] assumes that at any position along the pipe the flow rate can be approximated by its value in the linearized problem of

Table 7
Comparison of flow rate M_p and approximation (11) for $R_2/R_1 = 5$, 10.

	$R_2/R_1 = 5$				$R_2/R_1 = 10$			
δ_1	$L/R_1 = 10$	20	50	Eq. (11)	$L/R_1 = 10$	20	50	Eq. (11)
0.	4.789	6.890	9.331	12.547	5.54	9.69	16.01	27.42
0.1	4.789	6.998	9.380	11.916	5.64	9.88	16.24	26.02
1.	5.402	7.798	10.02	11.912	6.35	11.14	17.99	26.03
10.	7.601	12.78	19.00	23.646	8.18	15.40	30.45	52.30
100	8.650	16.90	39.72	159.19	8.73	17.26	41.88	355.09

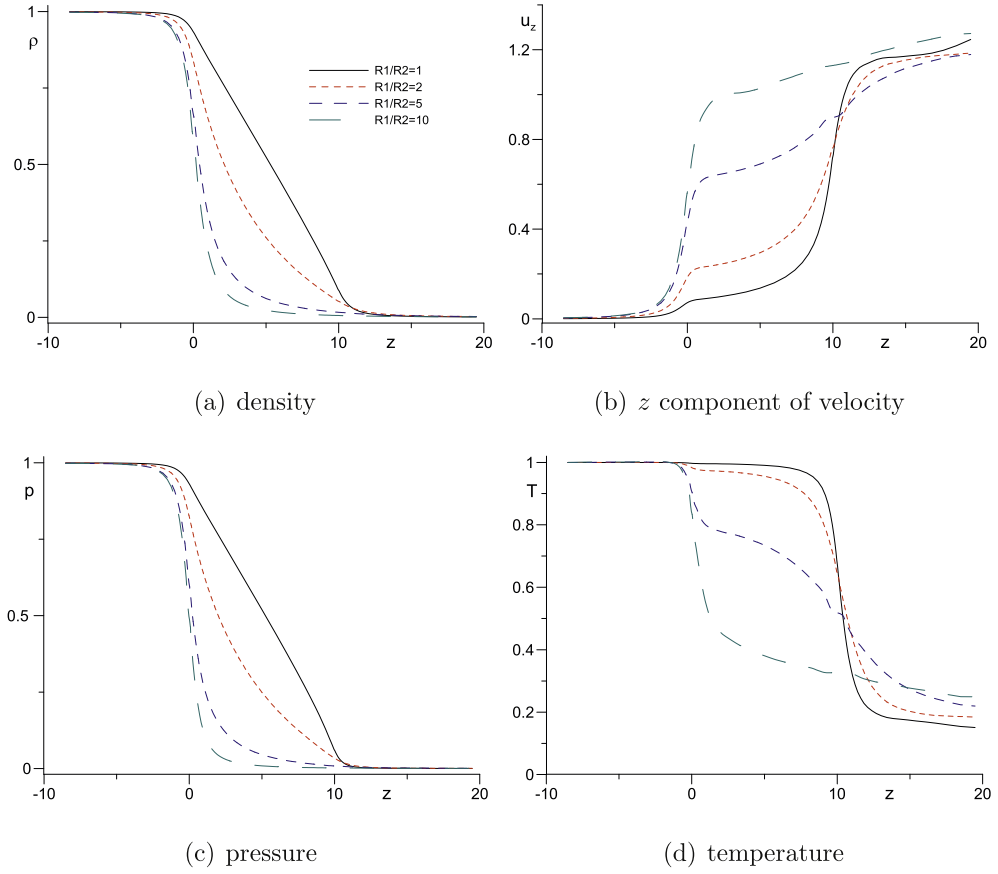

Fig. 2. Distribution of non-dimensional macroscopic quantities along the axial line for $L/R_1 = 10$ and $\delta_1 = 1$. (a) Density (b) z component of velocity (c) pressure (d) temperature.

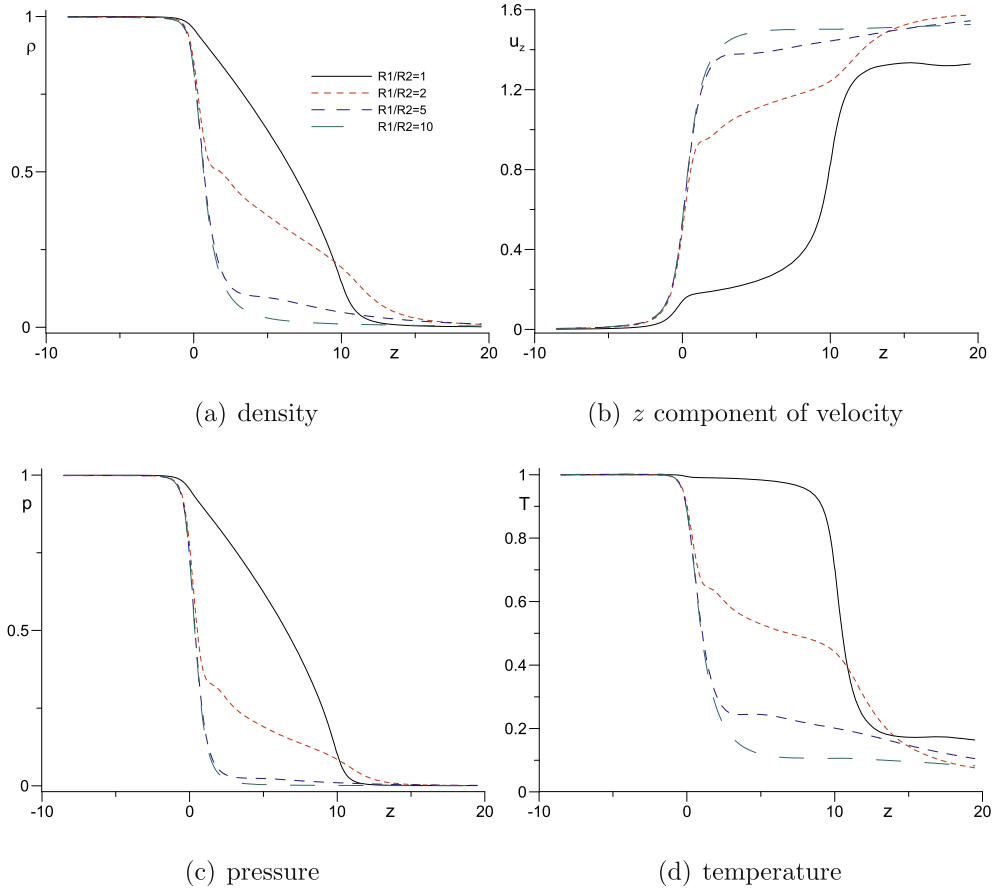

Fig. 3. Distribution of non-dimensional macroscopic quantities along the axial line for $L/R_1 = 10$ and $\delta_1 = 100$. (a) Density (b) z component of velocity (c) pressure (d) temperature.

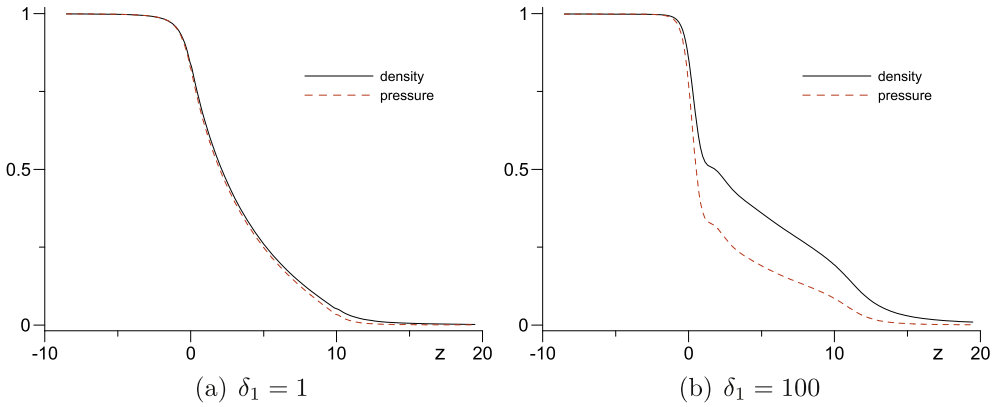

Fig. 4. Comparison of axial distributions of non-dimensional density and pressure for $L/R_1 = 10$, $R_2/R_1 = 2$. (a) $\delta_1 = 1$ (b) $\delta_1 = 100$.

gas flow in the infinitely long pipe. It is essential that the linearized solution is taken at the local value of the rarefaction parameter. In the case of the pressure-driven flow through a conical pipe the following approximate equation connects the flow rate M_p with the pressure gradient along the pipe [13]

$$M_p = -\frac{L}{p_1}\left(\frac{r(x)}{R_1}\right)^3 G_p(\delta(z))\frac{dp(z)}{dz}, \qquad r(z) = R_1 + (R_2 - R_1)\frac{z}{L}, \quad \delta(z) = \delta_1\frac{p(z)r(z)}{p_1 R_1}. \tag{11}$$

Here $G_p(\delta)$ is the flow rate for the case of the infinite pipe, see e.g. Ref. [2]. In the present work equation (11) is solved numerically using a second-order accurate marching method starting from the high-pressure reservoir. The sought approximate flow rate M_p is found from the condition that the computed pressure at $x = L$ be equal to the right reservoir pressure $p_2 = 0$.

Tables 6 and 7 show the comparison between the direct solution of the problem with the approximation (11) for $L/R_1 = 10$, 20 and 50. It is seen that there is visible discrepancy between the results even in the most favourable for the approximate method case of $L/R_1 = 50$, $R_2/R_1 = 1.1$. In other words, for the considered pipe's lengths the approximate method [13] for the conical pipe flow is significantly less accurate then for the constant radius circular pipe and the condition $\delta_1(R_1/L) \ll 1$ is no longer sufficient for it to be applicable.

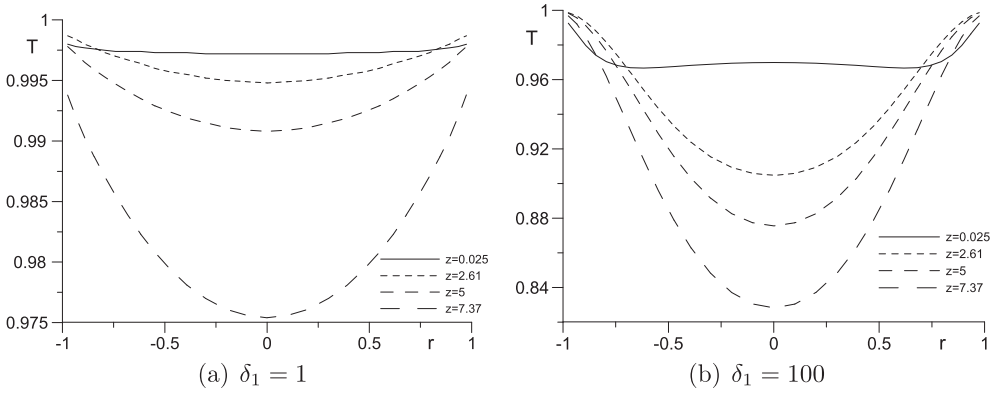

Fig. 5. Radial distribution of non-dimensional temperature for various z positions for $L/R_1 = 10$, $R_2/R_1 = 1$. (a) $\delta_1 = 1$ (b) $\delta_1 = 100$.

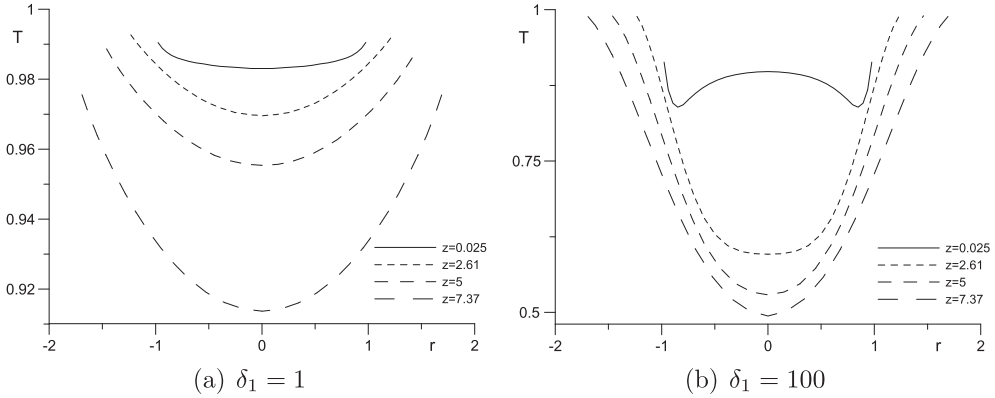

Fig. 6. Radial distribution of non-dimensional temperature for various z positions for $L/R_1 = 10$, $R_2/R_1 = 2$. (a) $\delta_1 = 1$ (b) $\delta_1 = 100$.

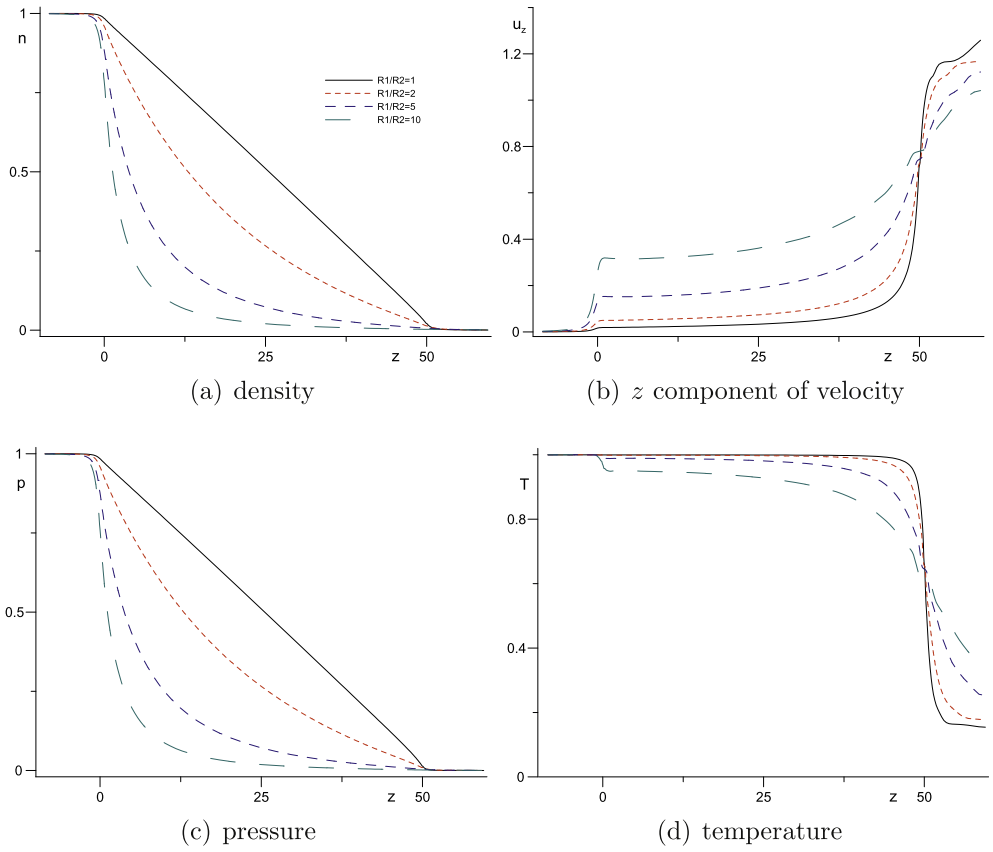

Fig. 7. Distribution of non-dimensional macroscopic quantities along the axial line for $L/R_1 = 50$ and $\delta_1 = 1$. (a) Density (b) z component of velocity (c) pressure (d) temperature.

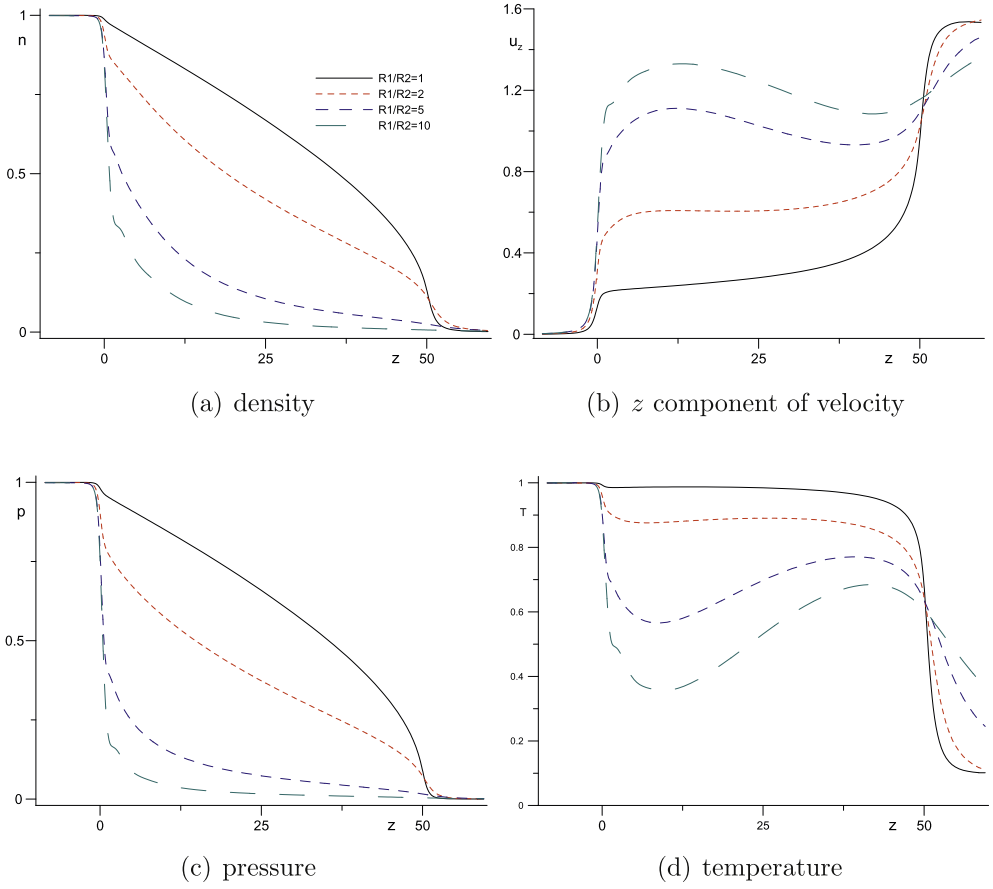

Fig. 8. Distribution of non-dimensional macroscopic quantities along the axial line for $L/R_1 = 50$ and $\delta_1 = 100$. (a) Density (b) z component of velocity (c) pressure (d) temperature.

The loss of accuracy of the approximate method is explained by the more complex flow pattern in the case of conical pipe. Indeed, at any section of the pipe the gas velocity is not generally directed along the z axis, as in the case of the constant pipe radius, but also has other components. Even for $L/R_1 = 50$ the flow pattern in the middle section of the pipe is thus quite complex and is not well approximated by the linearized solution. However, the accuracy of approximation (11) does improve as the pipe gets longer, so that one can expect, that for the sufficiently large value of the pipe length to outlet radius $L/R_2 \gg 1$ one can obtain reasonable results as long as δ_1 is not too large.

4.3. Flow field

Let us first consider the flow field for the case of the relatively short pipe $L/R_1 = 10$. Figs. 2 and 3 shows axial distributions of macroparameters for $\delta_1 = 1$ (rarefied regime) and $\delta_1 = 100$ (transitional/hydrodynamic regime) for all values R_2/R_1. It is seen that the variable cross section of the pipe significantly influences axial distributions, especially for $\delta_1 = 100$. For $R_2/R_1 = 2$ the pressure distribution deviates significantly from the linear dependence even for $\delta_1 = 1$. Gas temperature deviates from the constant value not only near the outlet, but also along the whole length of the pipe. The gas expansion and acceleration is most rapid for $R_2/R_1 \gg 1$, $\delta_1 \gg 1$ and is accompanied by large drop in temperature in almost entire pipe. Further illustration is provided on Fig. 4, which compares gas number density and pressure axial distributions for the case $R_2/R_1 = 2$. It is seen that although those almost coincide for the rarefied flow regime, in the transitional flow there is a visible difference.

Figs. 5 and 6 show radial temperature distributions for several positions along the pipe: $z = 0.025$ (close to inlet), 2.61 (approximately 25% of the length), 5 (middle) and 7.37 (approximately 75% of the length). The outlet position is excluded for the convenience of presentation. It is seen that for the circular pipe the temperature variation along the radius in the considered part of the pipe is quite small for both flow regimes so that the gas temperature is almost equal to the pipe's surface temperature. This is one of the key conditions for the construction of the axial solution on the basis of the asymptotic one, corresponding to the infinite pipe. However, for the conical pipe (see Fig. 6) the temperature departs very significantly from the surface one. This is especially evident for the case of transitional flow $\delta_1 = 100$.

Finally, Figs. 7 and 8 show axial distribution of macroscopic quantities for the longest considered pipe $L/R_1 = 50$. It is seen that the flow pattern is qualitatively similar to the case $L/R_1 = 10$, with the influence of the variable cross section clearly visible. However, the differences between circular and conical pipes are now smaller, which is expected. For $\delta_1 = 100$ the jump in temperature after the inlet is followed by a steady increase caused by heating from the pipe's surface. In the case of the shorter pipe $L/R_1 = 10$ this effect is not observed due to the insufficient lengths of the pipe.

5. Conclusions

Rarefied gas flow through a conical pipe into vacuum has been analysed numerically on the basis of the S-model kinetic equation. Flow rate for several length to radius ratios and outlet to inlet radii ratios has been computed. The results are compared with the constant-cross section circular pipe. It is shown that the variable (growing) pipe radius increases flow rates across all Knudsen numbers and as well as makes the flow pattern inside the pipe significantly nonlinear.

The presented results can be included in the recent set of benchmark problems in rarefied gas dynamics [7] and serve as reference data for calculations by other approaches, methods and codes.

Acknowledgements

This work was supported by the Russian Government under grant "On Measures to Attract Leading Scientists to Russian Educational Institutions" (contract No. 11.G34. 31.0072) and the Russian Foundation for Basic Research, project no. 13-01-00522. The use of the high-performance facilities of Lomonosov Moscow State University, Russia, is gratefully acknowledged.

References

[1] Koppenwallner G, Lips T, Dankert C. Discharge coefficients and on-axis flow properties in small sonic orifices at low Reynolds numbers. In: Ivanov MS, Rebrov AK, editors. Rarefied gas dynamics: 25-th International Symposium, Novosibirsk 2007. p. 585–91.
[2] Sharipov F, Seleznev V. Data on internal rarefied gas flows. J Phys Chem Ref Data 1998;27(3):657–706.
[3] Varoutis S, Valougeorgis D, Sazhin O, Sharipov F. Rarefied gas flow through short tubes into vacuum. J Vac Sci Technol 2008;26(1):228–38.
[4] Titarev V, Shakhov E. Computational study of a rarefied gas flow through a long circular pipe into vacuum. Vacuum, Special Issue "Vacuum Gas Dynamics: Theory, Experiments and Practical Applications" 2012;86(11):1709–16.
[5] Titarev V, Shakhov E. Rarefied gas flow through a long circular pipe into vacuum. In: Rarefied gas dynamics. Proc. 28th Int. Symp., AIP Conf. Proc. 1501 2012. p. 465–72.
[6] Titarev V, Shakhov E. End effects in the rarefied gas flow through a long pipe into vacuum. in press. Fluid Dyn 2013;(5).
[7] Sharipov F. Benchmark problems in rarefied gas dynamics. Vacuum, Special Issue "Vacuum Gas Dynamics: Theory, Experiments and Practical Applications" 2012;86(11):1697–700.
[8] Shakhov E. The axisymmetric non-linear steady flow of a rarefied gas in a pipe of circular cross section. Comput Math Math Phys 1996;36(8):1123–31.
[9] Larina I, Rykov V. A numerical method for calculating axisymmetric rarefied gas flows. Comput Math Math Phys 1998;38(8):1335–46.
[10] Akin'shin V, Makarov A, Seleznev V, Sharipov F. Flow of a rarefied gas in a plane channel of finite length for a wide range of Knudsen numbers. J Applied Mech Tech Phys 1988;29(1):97–103.
[11] Akin'shin V, Makarov A, Seleznev V, Sharipov F. Rarefied gas motion in a short planar channel over the entire Knudsen number range. J Applied Mech Tech Phys 1989;30(5):713–7.
[12] Sharipov F, Seleznev V. Rarefied gas flow through a long tube at any pressure ratio. J Vac Sci Technol A 1994;12(5):2933–5.
[13] Sharipov F, Bertoldo G. Rarefied gas flow through a long tube of variable radius. J Vac Sci Technol A 2005;23(3):531–3.
[14] Shakhov E. Approximate kinetic equations in rarefied gas theory. Fluid Dyn 1968;3(1):112–5.
[15] Shakhov E. Generalization of the Krook kinetic relaxation equation. Fluid Dyn 1968;3(5):95–6.
[16] Shakhov E. Kinetic model equations and numerical results. In: Proc. XIVth Intern. Symp. Rarefied gas dynamics. University of Tokyo Press; 1984. p. 137–48 [invited paper].
[17] Titarev V. Efficient deterministic modelling of three-dimensional rarefied gas flows. Commun Comput Phys 2012;12(1):161–92.
[18] Titarev V. Direct numerical solution of model kinetic equations for flows in arbitrary three-dimensional geometries. In: Rarefied gas dynamics. Proc. 28th Int. Symp., AIP Conf. Proc. 1501 2012. p. 262–71.
[19] Titarev V. Rarefied gas flow in a circular pipe of finite length. Vacuum 2013;94:92–103.
[20] Men'shov I, Nakamura Y. An implicit advection upwind splitting scheme for hypersonic air flows in thermochemical nonequilibrium. In: A collection of technical papers of 6th Int. Symp. on CFD, Vol. 2; 1995. p. 815. Lake Tahoe, Nevada.